

## RESEARCH ARTICLE

# Assessing the Carbon Sequestration Potential of Ultramafic Rocks in the Kolaka Ophiolite Complex, Southeastern Sulawesi: A Petrographic, Geochemical, and Mineralogical Study

Syahrul<sup>1,\*</sup>, La Ode Dzakir<sup>1</sup>, Riska<sup>1</sup>, Rio Irhan Mais Cendra Jaya<sup>2</sup>, Masri<sup>2</sup>

<sup>1</sup> Mining Engineering Department, Universitas Sembilanbelas November Kolaka, Southeast Sulawesi, Indonesia

<sup>2</sup> Geological Engineering Department, Halu Oleo University, Kendari, Southeast Sulawesi, Indonesia

\* Corresponding author : arulexplorer14@gmail.com

Tel.: 085241520475

Received: Oct 27, 2024; Accepted: Feb 10, 2024.

DOI: 10.25299/jgeet.2025.10.1.19484

## Abstract

Climate change has prompted significant global interest in carbon sequestration technologies, particularly using geological formations. This study investigates the potential of ultramafic rocks from the Kolaka Ophiolite Complex in Southeast Sulawesi for carbon sequestration, focusing on the mineralogical, petrographic, and geochemical characteristics that enhance their reactivity with CO<sub>2</sub>. The research involved petrographic and mineralogical analyses of 15 peridotite samples, geochemical measurements via X-ray fluorescence (XRF), and mineral characterization using scanning electron microscopy (SEM). The results revealed that Kolaka's ultramafic rocks, particularly harzburgite and lherzolite, exhibit moderate to high serpentinization, which enhances their reactivity with CO<sub>2</sub>. Key minerals such as olivine, pyroxene, and serpentine, rich in magnesium, calcium, and iron oxides, demonstrate significant potential for mineral carbonation. Secondary minerals like magnesite and brucite were identified as products of carbonation, reinforcing the rocks' ability to act as carbon sinks. The discussion highlights that serpentinized peridotites are more effective for carbon sequestration than unaltered ones due to increased mineral reactivity. The presence of magnesite and Cr-Fe-rich carbonates, alongside serpentine veins, indicates that fluid-rock interactions have promoted ongoing carbonation processes. The Kolaka ultramafic rocks, therefore, hold strong potential for long-term carbon storage, offering a promising solution for reducing atmospheric CO<sub>2</sub> levels.

**Keywords:** Carbon Sequestration, Degree Of Serpentinization, Mineral Carbonation, Peridotite, Kolaka

## 1. Introduction

Climate change is generally defined as a significant shift in weather patterns over an extended period, ranging from several decades to millions of years. It is caused by various factors, including human activities and natural variability (Medhaug et al., 2017), which greatly impact Earth's ecosystems and the economy. Climate change also significantly affects geological processes, influencing various aspects of Earth's systems. Geological factors such as tectonic activity drive climate change, impacting topographic changes, glaciation, flora evolution, the hydrological cycle, and carbon sequestration (Triana and Wahyudi, 2020). There is a recognized link between climate change and geological hazards. Global climate change, seismic activity, and the acceleration of urbanization lead to an increase in significant geological disasters such as landslides and floods (Chang et al., 2022). Additionally, the impact of climate change on rising sea levels can be influenced by geological processes like land subsidence. Therefore, an integrated assessment of the consequences of climate change is crucial, as these effects transcend sectoral and regional boundaries and influence hydrological and geological behaviors in various aspects (Trivedi et al., 2019).

The Paris Agreement, established under the United Nations Framework Convention on Climate Change (UNFCCC), represents a significant global effort to combat climate change. This agreement involves 194 member countries committed to limiting the rise in global average temperature to below 2°C above pre-industrial levels, with efforts to cap it at 1.5°C above pre-industrial levels (Asadnabizadeh, 2019). The key element

of the Paris Agreement is the paradigm of sustainable development in controlling climate change. The agreement also emphasizes the need for significant global investments to support climate change mitigation and adaptation efforts (Tolliver et al., 2019). However, current projections suggest that Earth's temperature may not align with the targets outlined in the Paris Agreement (Höhne et al., 2021), (Rogelj et al., 2016), necessitating more aggressive and ambitious efforts, including accelerating carbon emission reductions.

Carbon Capture and Storage (CCS) is a crucial technology for reducing anthropogenic carbon dioxide emissions (Matter et al., 2016). Carbon storage is necessary to ensure the ongoing efficiency of the natural carbon cycle. In marine environments, seagrass meadows and certain types of seaweed contribute effectively to carbon sequestration (Erlania et al., 2013). On land, mangrove forests are recognized as one of the most efficient ecosystems for fixing atmospheric carbon dioxide and storing it in biomass and sediments (Jompa and Murdiyarso, 2022). Studies on the geological components of carbon storage media have also been conducted. These studies typically focus on rocks with high porosity and permeability, commonly found in deep marine aquifers, hydrocarbon reservoirs, coal seams, and carbonate basins (Luu et al., 2022), (Tutolo et al., 2014), (Warwick and Zhu, 2012). Karst morphologies are also considered effective traps for carbon dioxide absorption during carbonate dissolution (Punnam et al., 2022).

Recent studies suggest the potential of ultramafic rocks as carbon storage media (Snæbjörnsdóttir et al., 2020). Ultramafic rocks, such as peridotite, composed primarily of minerals like

olivine and pyroxene, are rich in calcium, magnesium, and iron oxides, all of which exhibit high reactivity in the carbonation process (Kelemen et al., 2020),(Andreani et al., 2009). Magnesium can react with CO<sub>2</sub> gas to form carbonate minerals and silica (Bide et al., 2014). In serpentinized ultramafic rocks, increased mineral reactivity towards CO<sub>2</sub> absorption has also been observed (Snæbjörnsdóttir et al., 2020). Several minerals, such as olivine, serpentine, brucite, wollastonite, and anorthite-rich plagioclase, display high reactivity with CO<sub>2</sub> gas (Irzon et al., 2024), which transforms into hydrated magnesium carbonate minerals like magnesite and nesquehonite (Harrison et al., 2018).

The Southeastern Sulawesi Arm contains a vast spread of ultramafic complexes, particularly in the Kolaka region (Kadarusman et al., 2004),(Simandjuntak et al., 1993). Unlike the Eastern Sulawesi Ophiolite (ESO), this complex tends to appear with an incomplete ophiolite sequence (Maulana et al., 2015),(Kadarusman et al., 2004). The ultramafic rocks are well exposed in hills, ridges, and nickel laterite mining pits. These fractured ultramafic exposures can be a media for in-situ or ex-situ carbon sequestration and storage. Studies on the potential of ultramafic complexes for CCS have been conducted in the Meratus Ultramafic Complex (Irzon et al., 2024) and Central Sulawesi Ultramafic Complex (Sufriadin et al., 2020).

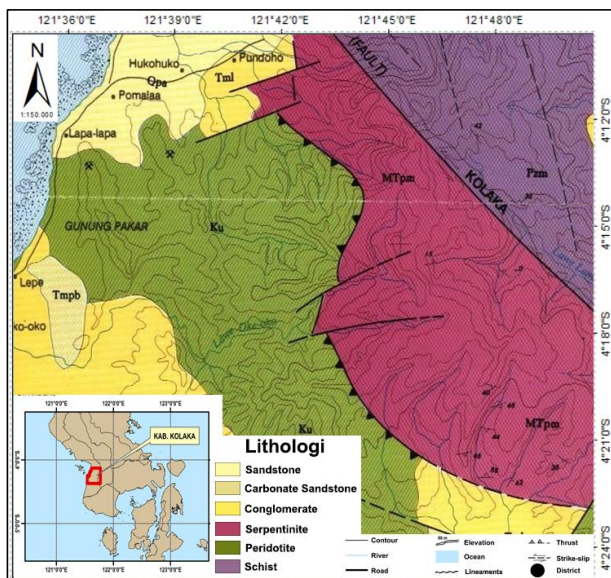


Fig. 1 Geological map of Kolaka Region (modified from (Simandjuntak et al., 1993))

These studies generally focus on the oxide composition of rocks and the correlation between the degree of serpentinization and the mineralogy of key compounds that affect the potential of rocks as carbon sequestration media. The characteristics of the Kolaka Ultramafic Complex differ from those of the Meratus and Central Sulawesi complexes, offering the potential for unique carbon sequestration analysis. Unlike previous research, this study emphasizes mineral chemistry in ultramafic rocks. This study focuses on the characteristics of ultramafic rocks in the Kolaka region and their potential for carbon sequestration and storage (Fig. 1). The characteristics include mineralogical features, oxide compound content, and mineral chemistry. The mineralogy emphasizes the presence of primary minerals that easily undergo carbonation reactions, such as olivine, serpentine, and brucite. The presence of secondary minerals produced through carbonation, like dolomite and magnesite, is also a research focus. Oxide compound content is intended to determine the percentage of calcium, magnesium, and iron oxides at various levels of serpentinization in ultramafic rocks. Mineral chemistry aims to identify olivine,

pyroxene, and serpentine types with the highest magnesium fraction, such as magnesium-rich olivine, pyroxene, and serpentine.

## 2. Methodology

The research methodology comprises several stages, including data collection, petrographic and mineragraphic observation of thin sections, measurement of major compounds in bulk rock samples, determination of potential carbonation mineral composition, and data analysis and synthesis. Geological mapping and the distribution of ultramafic rocks in the Kolaka Ophiolite Complex have been conducted by Jaya et al. (2024b). There are approximately 200 km<sup>2</sup> of ultramafic rock distribution has been identified in the Kolaka Ophiolite Complex (Syahrul, 2017, Simandjuntak et al., 1993).

In this study, data has been collected from 15 representative peridotite rock samples from Kolaka Regency, Southeast Sulawesi. The rock samples then have been prepared for analysis. The analyses included microscopic observations (petrography and mineragraphy), geochemical measurements using X-Ray Fluorescence (XRF), and further microscopic observations using a Scanning Electron Microscope (SEM) equipped with an Energy Dispersive X-Ray Spectroscopy (EDS) detector. Petrographic and mineragraphic analyses have been conducted on 15 thin-section and polished rock samples using a polarizing microscope in both reflection and refraction modes. These observations aim to identify the constituent minerals of the rocks based on their optical properties. The focus is on identifying minerals and characteristic mineral textures associated with the carbonation process, such as the presence of metal minerals or magnesium-rich alteration minerals (e.g., magnesite). Additionally, observations focus on determining the degree of serpentinization. These observations classify the rock samples according to carbonation intensity and alteration/serpentinization degree. Measurement of major compounds in bulk rock samples following the classification of data based on microscopic observations, the geochemical composition of the rocks have been determined using X-Ray Fluorescence (XRF) spectrometry. The XRF analysis aimed to identify the major chemical oxide compounds in the rocks, focusing on calcium, magnesium, silica, and iron oxide content. The rock samples, previously classified based on carbonation intensity and alteration, had been prepared as compacted pellets (pressed pellets) after being ground to a size of #200 mesh. The major compound measurements were performed on each sample's rock pellet. Determination of potential carbonation mineral composition is based on petrographic/mineragraphic observations and chemical oxide data. Further microscopic observation uses Scanning Electron Microscopy (SEM), complemented by Energy Dispersive X-Ray Spectroscopy (EDS). The purpose of the SEM-EDS analysis is to determine the characteristics, composition, and chemical content of specific minerals that have the potential for carbon sequestration based on the XRF and petrographic/mineragraphic analyses. The potential carbonation minerals include olivine, pyroxene, serpentine, brucite, wollastonite, and alteration minerals such as magnesite (Irzon et al., 2024), (Sufriadin et al., 2020), (Kelemen et al., 2019). The results of the three analyses will be synthesized by the researchers to determine the potential of ultramafic rocks in the Kolaka Ophiolite Complex for carbon absorption and storage. The mineral characteristics, major chemical oxide data, and potential carbonation mineral data will be used to interpret the carbon absorption potential of the rocks. The synthesis will include the correlation between the abundance of carbonation minerals and the rock texture and degree of alteration/serpentinization. The distribution of ultramafic rock lithology also synthesized with the available chemical data.

### 3. Results

#### 3.1 Petrography of Peridotite Rocks

The ultramafic rocks in the Kolaka Ophiolite Complex are peridotites that have undergone moderate to high degrees of serpentinization (Fig. 2). Based on the analysis of 15 thin sections of peridotite from the study area and following Streckeisen's classification (1976), the peridotite rocks are divided into harzburgite and lherzolite.

Harzburgite in the study area consists of olivine (50–70%), orthopyroxene (15–30%), clinopyroxene (5–15%), and chromite-spinel (<5%). Lherzolite comprises olivine (40–50%), orthopyroxene (20–30%), clinopyroxene (25–30%), and chromite-spinel (<5%). Lherzolite exhibits a higher degree of serpentinization than harzburgite, determined through visual petrographic observations (Fig. 2). The development of hourglass and interlocking serpentine textures (Fig. 2b) also

indicate moderate to high degrees of serpentinization (Jaya et al., 2024a). The secondary minerals present in peridotite rocks due to alteration, carbonation, and other processes are listed in Table 1. The peridotite rocks are primarily composed of olivine and pyroxene, rich in calcium, magnesium, and iron oxides and serpentinized, which exhibit high reactivity in carbonation processes (Kelemen et al., 2020), (Andreani et al., 2009). Magnesium content, in particular, reacts with CO<sub>2</sub> to form carbonate and silica minerals (Bide et al., 2014). In serpentinized peridotite rocks, increased mineral reactivity towards CO<sub>2</sub> absorption has been observed (Snæbjörnsdóttir et al., 2020), (Power et al., 2013). Minerals such as olivine, serpentine, and brucite show high reactivity with CO<sub>2</sub>, transforming into hydrated magnesium carbonates like magnesite and nesquehonite (Irzon et al., 2024), (Harrison et al., 2018).

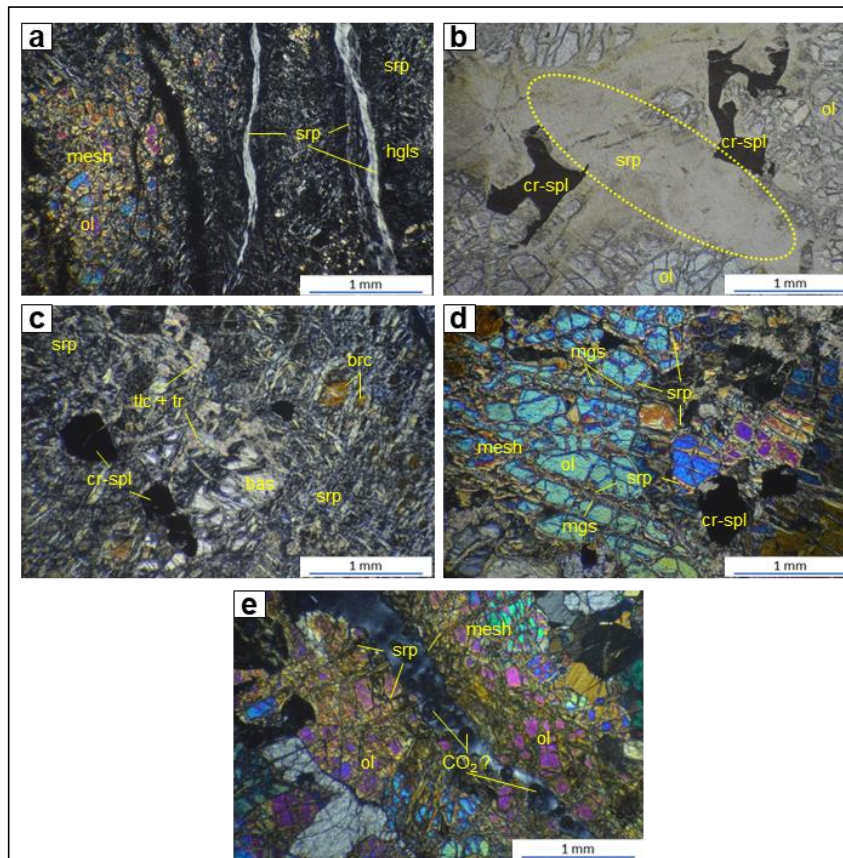


**Fig. 2** Microphotographs of several peridotite rock thin sections in cross-polarized light (a, c, d, and e) and plane-polarized light (b). (a) Harzburgite OKO-01p exhibits moderate to high degrees of serpentinization with mesh and hourglass textures. Serpentine fills the fractures in the olivine. (b) Harzburgite OKO-03p displays the development of interlocking texture (indicated by yellow ovals) in serpentine. Chromite-spinel shows intergrowth textures with olivine. (c) Lherzolite GBA-02p demonstrates a high degree of serpentinization, where bastite (serpentine group) replaces the pyroxene associated with chromite-spinel, exhibiting hourglass texture in the rock section. The development of hourglass and interlocking textures indicates that serpentinization has progressed to a more advanced stage [9]. Brucite is identified as replacing olivine, while talc and tremolite are observed to develop on the rims of pyroxene and chromite-spinel. (d) Harzburgite OKO-04p shows olivine cumulate intergrowth with serpentinized chromite-spinel. Serpentine forms a mesh texture. Magnesite is identified to crystallize around the serpentine vein as a carbonation mineral. (e) Harzburgite OKO-04p displays an olivine cumulate that is fragmented by serpentine mesh. A fracture is present in the center of the section filled with gas (bubbles) CO<sub>2</sub>, which is trapped. This fracture represents secondary porosity cutting through the olivine crystals and serpentine vein, interpreted to have formed after the serpentinization or during the carbonation process.

#### 3.2 The Whole-Rock Analysis of Peridotite Rocks

Major oxide compounds in peridotite rocks were analyzed using X-ray fluorescence (XRF) spectrometry, focusing on calcium, magnesium, silica, and iron oxide content. Samples were prepared as pressed pellets, ground to #200 mesh, to measure major compounds in the bulk rock.

The whole-rock major element analysis revealed high concentrations of SiO<sub>2</sub> and MgO, indicating that the peridotite rocks are rich in silica and magnesium (Table 2). Magnesium-rich minerals such as olivine, pyroxene, magnesite, brucite, and serpentine play crucial roles in carbon absorption and storage, warranting detailed mineral chemical characterization.

#### 3.3 Potential Carbon Sequestration Mineral Chemistry

The olivine present is predominantly forsterite, with higher magnesium (Mg) content than iron (Fe). Some olivine crystals displayed increased silica content, indicative of intensive serpentinization processes. The pyroxene minerals present in the rock comprise both clinopyroxene and orthopyroxene. All identified orthopyroxenes are enstatite (Table 3), characterized by a high magnesium (Mg) content (>30%). The clinopyroxene is represented by diopside (OKO-04p and GBA-01p), which exhibits high calcium (Ca) and magnesium (Mg) contents, and

pigeonite (OKO-06p), characterized by elevated magnesium (Mg) and iron (Fe) contents but low calcium (Ca) levels. The reduced Ca content in clinopyroxene is interpreted as a result of exsolution processes occurring between pyroxene crystals (Jaya et al., 2024b). Another magnesium-rich mineral identified is brucite (Fig. 3), which has an Mg content exceeding 70%. Brucite (GBA-02p) is present as a mineral that alters olivine. Additionally, manganese oxide (WOL-02p), rich in magnesium, is found within the peridotite rock.

Table 1. Representation of minerals from 15 thin sections of peridotite. Mineral symbols based on Whitney and Evans (2009)

| Sample  | Primary Minerals       | Secondary Minerals        | Intensity of serpentinization | Lithology  |
|---------|------------------------|---------------------------|-------------------------------|------------|
| OKO-01P | Ol + Opx + Cpx +Cr-Spl | Srp + mag                 | 70 – 80%                      | Harzburgit |
| OKO-02P | Ol + Opx + Cpx         | Srp + mag                 | 60 – 70%                      | Harzburgit |
| OKO-03P | Ol + Opx + Cpx +Cr-Spl | Srp + mag                 | 60 – 70%                      | Harzburgit |
| OKO-04P | Ol + Opx + Cpx +Cr-Spl | Srp + mgs +cb             | 70 – 80%                      | Harzburgit |
| OKO-05P | Ol + Opx + Cpx         | Srp                       | 50 – 60%                      | Harzburgit |
| OKO-06P | Ol + Opx + Cpx +Cr-Spl | Srp +mgs + cb             | 50 – 60%                      | Harzburgit |
| GBA-01P | Ol + Opx + Cpx +Cr-Spl | Srp + cal +qz             | 60 – 70%                      | Lerzolit   |
| GBA-02P | Ol + Opx + Cpx         | Srp +mgs + brc + tlc + tr | 70 – 80%                      | Lerzolit   |
| GBA-03P | Ol + Opx + Cpx         | Srp +cal                  | 70 – 80%                      | Lerzolit   |
| GBA-04P | Ol + Opx + Cpx +Cr-Spl | Srp + tlc + tr            | 70 – 80%                      | Lerzolit   |
| GBA-05P | Ol + Opx + Cpx         | Srp + tlc + tr            | 60 – 70%                      | Lerzolit   |
| WOL-01P | Ol + Opx + Cr-Spl      | Srp                       | 60 – 70%                      | Harzburgit |
| WOL-02P | Ol + Opx + Cr-Spl      | Srp +mn oxide             | 50 – 60%                      | Harzburgit |
| WOL-03P | Ol + Opx + Cpx+ Cr-Spl | Srp                       | 50 – 60%                      | Harzburgit |
| WOL-04P | Ol + Opx + Cpx+ Cr-Spl | Srp                       | 50 – 60%                      | Harzburgit |

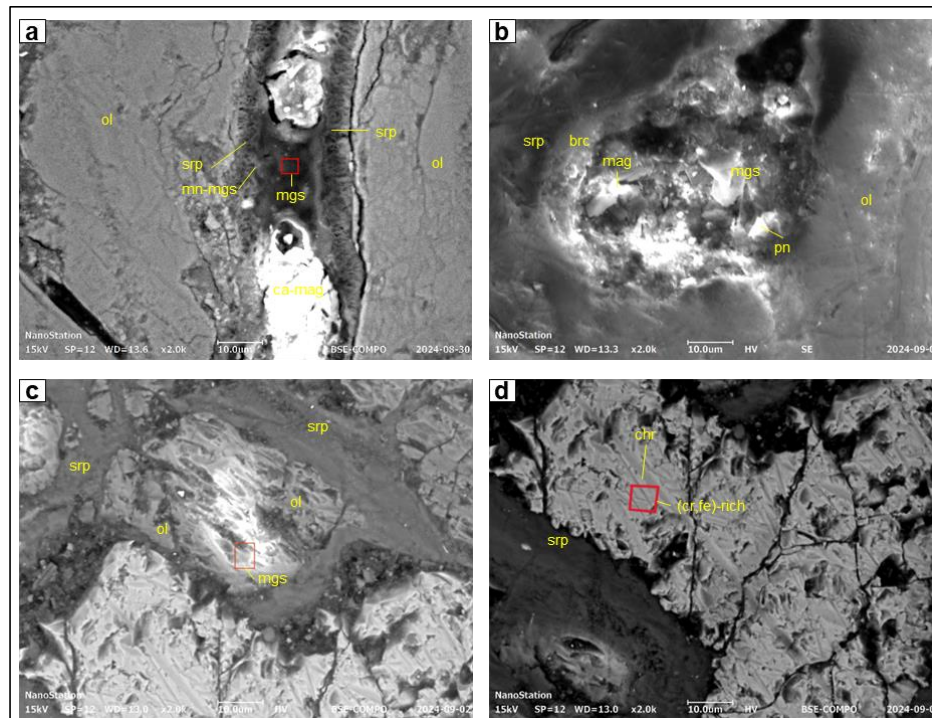


Fig. 3 Observations using SEM on polished sections of peridotite rock. (a) The serpentine-magnesium vein within olivine, with magnetite, is also found to be associated with the serpentine-magnesium vein. (b) Hydration of olivine minerals crystallizes brucite, magnesite, and serpentine at the rims of olivine. Magnetite and pentlandite are also identified. (c) Carbonation occurs in serpentinized olivine, resulting in the formation of magnesite. (d) Carbonation in chromite-spinel leads to the production of carbonate minerals rich in chromium (Cr) and iron (Fe)

Table 2 Major chemical compounds of peridotite rocks in the study area

| Sample                         | GBA-01p | GBA-02p | GBA-03p | WOL-02p | WOL-03p | OKO-02p | OKO-03p | OKO-04p | OKO-05p | OKO-06p |
|--------------------------------|---------|---------|---------|---------|---------|---------|---------|---------|---------|---------|
| MgO                            | 43,559  | 43,719  | 44,402  | 40,172  | 43,513  | 46,597  | 41,004  | 46,237  | 45,377  | 46,364  |
| Al <sub>2</sub> O <sub>3</sub> | 1,318   | 1,183   | 1,654   | 2,232   | 1,436   | 0,454   | 1,228   | 0,827   | 0,791   | 0,69    |
| SiO <sub>2</sub>               | 39,959  | 37,54   | 34,713  | 38,524  | 36,932  | 37,249  | 32,868  | 34,772  | 37,062  | 35,301  |
| CaO                            | 0,143   | 0,921   | 0,859   | 1,423   | 0,827   | 0,062   | 3,548   | 0,543   | 0,085   | 0,527   |
| TiO <sub>2</sub>               | 0,01    | 0,01    | 0,012   | 0,017   | 0,013   | 0,006   | 0,006   | 0,008   | 0,006   | 0,007   |
| Cr <sub>2</sub> O <sub>3</sub> | 0,34    | 0,269   | 0,231   | 0,208   | 0,281   | 0,243   | 0,179   | 0,262   | 0,265   | 0,238   |
| MnO                            | 0,068   | 0,109   | 0,074   | 0,069   | 0,072   | 0,06    | 0,077   | 0,07    | 0,077   | 0,068   |
| Fe <sub>2</sub> O <sub>3</sub> | 4,067   | 4,211   | 4,564   | 4,338   | 4,49    | 3,927   | 4,437   | 4,429   | 4,598   | 4,195   |
| Co                             | 0,021   | 0,02    | 0,021   | 0,019   | 0,021   | 0,021   | 0,016   | 0,021   | 0,022   | 0,021   |
| Ni                             | 0,117   | 0,122   | 0,132   | 0,121   | 0,129   | 0,12    | 0,135   | 0,139   | 0,151   | 0,126   |

**Table 3.** Chemical representation of olivine, clinopyroxene, orthopyroxene, Mn-oxide, brucite, and quartz

| Sampel Minerals                | OKO-02p      | OKO-04p       | GBA-03p       | WOL-02p      | OKO-04p      | GBA-02p       | WOL-02p      | GBA-02p      | GBA-01p      |
|--------------------------------|--------------|---------------|---------------|--------------|--------------|---------------|--------------|--------------|--------------|
|                                | Olivine      |               |               |              | Cpx          | Opx           | Mn-Oxide     | Brucite      | Quartz       |
| SiO <sub>2</sub>               | 39,10        | 40,60         | 45,27         | 63,15        | 53,16        | 59,59         | 21,66        | 13,09        | 78,67        |
| TiO <sub>2</sub>               | 0,02         | 0,17          | 0,00          | 0,06         | 0,07         | 0,15          | 0,00         | 0,00         | 0,00         |
| Al <sub>2</sub> O <sub>3</sub> | 0,28         | 0,21          | 2,99          | 0,12         | 1,91         | 0,46          | 0,10         | 0,67         | 0,70         |
| FeO                            | 2,39         | 4,10          | 7,88          | 0,33         | 2,26         | 4,41          | 2,95         | 0,45         | 1,67         |
| MnO                            | 0,05         | 0,13          | 0,13          | 0,15         | 0,14         | 0,11          | 34,75        | 0,02         | 0,01         |
| MgO                            | 55,43        | 54,46         | 41,87         | 35,84        | 23,21        | 33,18         | 25,24        | 80,05        | 16,83        |
| CaO                            | 0,10         | 0,00          | 0,27          | 0,03         | 15,59        | 0,83          | 0,18         | 3,61         | 0,78         |
| Na <sub>2</sub> O              | 0,22         | 0,00          | 0,14          | 0,00         | 0,19         | 0,06          | 0,04         | 0,00         | 0,19         |
| K <sub>2</sub> O               | 0,04         | 0,02          | 0,03          | 0,00         | 0,05         | 0,05          | 0,03         | 0,00         | 0,28         |
| Cr <sub>2</sub> O <sub>3</sub> | 0,09         | 0,12          | 0,59          | 0,00         | 0,31         | 0,03          | 0,00         | 0,02         | 0,06         |
| CoO                            | 0,13         | 0,27          | 0,13          | 0,00         | 0,05         | 0,31          | 0,70         | 0,00         | 0,00         |
| NiO                            | 0,00         | 0,20          | 0,23          | 0,00         | 0,69         | 0,45          | 0,80         | 0,01         | 0,14         |
| ZnO                            | 0,24         | 0,36          | 0,47          | 0,21         | 0,52         | 0,55          | 0,00         | 0,06         | 0,46         |
| V <sub>2</sub> O <sub>3</sub>  | 0,00         | 0,11          | 0,00          | 0,10         | 0,00         | 0,00          | 0,00         | 0,00         | 0,05         |
| <b>Total</b>                   | <b>98,08</b> | <b>100,75</b> | <b>100,01</b> | <b>99,98</b> | <b>98,15</b> | <b>100,20</b> | <b>86,45</b> | <b>97,98</b> | <b>99,85</b> |

**Table 4.** Chemical representation of magnesite, (Cr, Fe)-rich carbonate, and calcite

| Sample Minerals   | OKO-04p       | OKO-06p       | GBA-02p       | OKO-06p                 | GBA-01p       |
|-------------------|---------------|---------------|---------------|-------------------------|---------------|
|                   | Magnesite     |               |               | (Cr, Fe)-rich Carbonate | Calcite       |
| MgCO <sub>3</sub> | 77,32         | 70,54         | 76,67         | 68,57                   | 4,54          |
| CaCO <sub>3</sub> | 4,08          | 9,57          | 5,11          | 1,18                    | 87,40         |
| MnCO <sub>3</sub> | 2,04          | 1,15          | 2,56          | 9,79                    | 0,00          |
| FeCO <sub>3</sub> | 4,49          | 9,54          | 5,62          | 9,76                    | 4,17          |
| SrCO <sub>3</sub> | 0,00          | 0,00          | 0,05          | 0,00                    | 0,29          |
| AlCO <sub>3</sub> | 10,62         | 9,20          | 8,18          | 9,42                    | 4,96          |
| CrCO <sub>3</sub> | 1,44          | 0,00          | 1,80          | 1,28                    | 0,02          |
| <b>Total</b>      | <b>100,00</b> | <b>100,00</b> | <b>100,00</b> | <b>100,00</b>           | <b>101,39</b> |

**Table 5.** Chemical representation of serpentine

| Sampel Minerals                | WOL-02p      |              |              | GBA-02p      |              |              |              |
|--------------------------------|--------------|--------------|--------------|--------------|--------------|--------------|--------------|
|                                | Serpentine   |              |              |              |              |              |              |
| SiO <sub>2</sub>               | 53,57        | 53,73        | 41,71        | 44,40        | 50,74        | 47,68        | 46,15        |
| TiO <sub>2</sub>               | 0,00         | 0,00         | 0,01         | 0,01         | 0,01         | 0,01         | 0,01         |
| Al <sub>2</sub> O <sub>3</sub> | 0,47         | 0,33         | 0,35         | 0,41         | 0,23         | 0,21         | 0,23         |
| FeO                            | 2,84         | 1,75         | 11,91        | 7,43         | 6,86         | 6,24         | 9,71         |
| MnO                            | 0,03         | 0,03         | 0,57         | 0,26         | 0,23         | 0,21         | 0,23         |
| MgO                            | 35,28        | 33,18        | 32,14        | 29,61        | 32,58        | 38,77        | 32,22        |
| CaO                            | 0,11         | 0,11         | 0,59         | 0,51         | 0,36         | 0,48         | 0,53         |
| Na <sub>2</sub> O              | 0,00         | 0,00         | 0,07         | 0,03         | 0,02         | 0,06         | 0,03         |
| K <sub>2</sub> O               | 0,00         | 0,00         | 0,00         | 0,00         | 0,00         | 0,00         | 0,00         |
| Cr <sub>2</sub> O <sub>3</sub> | 0,42         | 0,43         | 0,11         | 0,54         | 0,49         | 0,72         | 0,90         |
| CoO                            | 0,11         | 0,11         | 0,73         | 0,01         | 0,09         | 0,09         | 0,06         |
| NiO                            | 0,21         | 0,22         | 0,54         | 0,50         | 0,50         | 0,50         | 0,59         |
| ZnO                            | 0,11         | 0,11         | 0,85         | 0,04         | 0,04         | 0,03         | 0,02         |
| V <sub>2</sub> O <sub>3</sub>  | 0,00         | 0,00         | 0,21         | 0,02         | 0,05         | 0,05         | 0,06         |
| <b>Total</b>                   | <b>93,15</b> | <b>90,00</b> | <b>89,78</b> | <b>83,77</b> | <b>92,22</b> | <b>95,06</b> | <b>90,73</b> |

Based on the mineral chemical data on Table 4, the identified carbonate minerals are magnesite, (Cr, Fe)-rich carbonates, and calcite. Magnesite is associated with secondary minerals such as serpentine, brucite, and talc within veins or rims of olivine, pyroxene, or chromite-spinel (Fig. 3). The presence of magnesite is attributed to carbonation processes occurring in the peridotite rock. Additionally, manganese-rich magnesite (Mn) was identified in sample GBA-02p. The transformation of serpentinized peridotite due to carbonation results in the formation of magnesite, other carbonate minerals, relic chromite-spinel, and quartz. Other carbonate minerals identified include calcite and chromium- (Cr) and iron- (Fe) rich carbonates (Table 4). Calcite is typically present as veins. The presence of chromium- and iron-rich carbonates is interpreted to result from reactions between chromite-spinel and carbonating fluids (Fig. 3d). Quartz was found in sample GBA-01p in the form of veins, interpreted as a product of the high degree of carbonation by a CO<sub>2</sub>-bearing fluid that may result in either excess Si and Fe or removal of both Si and Fe from the system (Hansen et al., 2005). Serpentine minerals

present generally exhibit a homogeneous chemical composition with high magnesium (Mg) content.

#### 4. Discussion

The petrographic and geochemical analyses of peridotite samples from the Kolaka Ophiolite Complex indicate significant serpentinization, especially in lherzolite, which shows higher degrees of alteration than harzburgite. Serpentinization enhances the reactivity of minerals such as olivine and pyroxene, increasing their potential for carbonation and carbon sequestration (Rigopoulos et al., 2018). The presence of magnesium-rich minerals, such as forsterite (olivine) and enstatite (orthopyroxene), along with secondary minerals like magnesite and calcite (Snæbjörnsdóttir et al., 2020), further supports that these rocks can act as effective carbon sinks through mineral carbonation processes. A higher degree of serpentinization further increases serpentinization intensity and accelerates the carbonation process (Fig. 4). Magnesite with higher CO<sub>3</sub> content thus crystallizes, replacing serpentine. Some (Cr, Fe)-rich carbonates also recrystallize

from Cr-spinel. Rare calcite suggests the infiltration of CO<sub>2</sub> + Ca-bearing fluid (Steinthorsdottir et al., 2022).

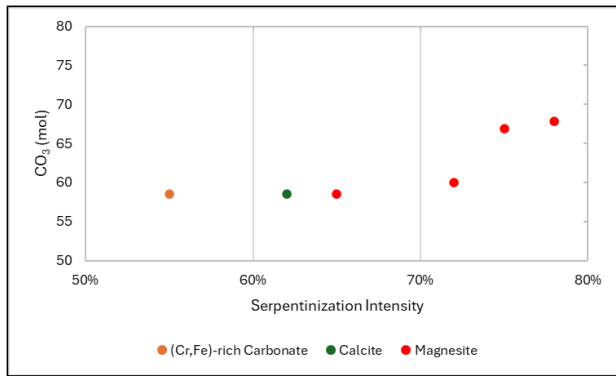


Fig. 4 CO<sub>3</sub> changes in carbonate minerals with progressive serpentinization

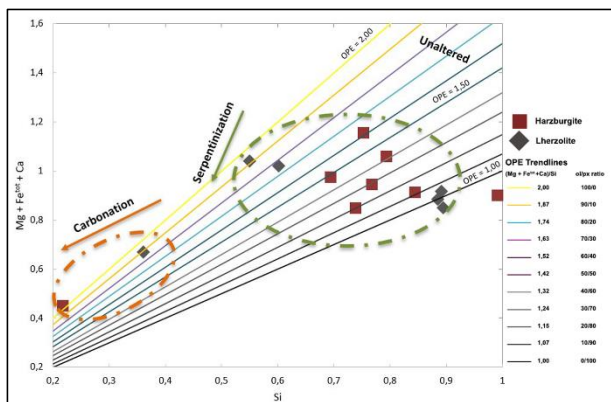


Fig. 5 Major element changes with progressive serpentinization and carbonation

The molar ratio of (Mg + Fe<sup>tot</sup> + Ca)/Si, referred to by Steinhorsdottir et al. (2022) as an olivine-pyroxene elemental ratio (OPE), shows the change in major element composition during serpentinization. Fig. 5 shows that the carbonation of peridotite is the continuation of serpentinization. Serpentinized peridotite will provide better carbon sequestration than unaltered peridotite. The geochemical data reveal high levels of MgO and SiO<sub>2</sub>, highlighting the potential of serpentinized peridotites in carbon storage. The magnesium content in these minerals is particularly crucial because it reacts with CO<sub>2</sub> to form stable carbonate minerals such as magnesite and brucite (Sufriadin et al., 2020). The presence of secondary minerals like talc and serpentine in association with magnesite suggests that carbonation processes are ongoing, with serpentinized fractures providing pathways for CO<sub>2</sub> to react with the host rock. This process not only immobilizes CO<sub>2</sub> but also contributes to porosity development, further facilitating carbon sequestration. The identification of Cr-Fe-rich carbonates, in conjunction with calcite and quartz, suggests that the peridotites have undergone complex carbonation and alteration processes. These reactions indicate that the peridotite formations in the Kolaka region are well-suited for long-term CO<sub>2</sub> storage. The observed association of carbonate minerals with serpentine veins suggests that fluid-rock interactions played a vital role in mineralizing carbon, making these formations promising targets for enhanced geological carbon storage initiatives.

## 5. Conclusion

The results reveal that the peridotite rocks in the Kolaka region, specifically harzburgite and lherzolite, contain significant amounts of olivine, pyroxene, and serpentine,

minerals known for their high reactivity with CO<sub>2</sub>. The study highlights that the Kolaka peridotite rocks, characterized by their high magnesium content and significant degrees of serpentinization, demonstrate strong potential for carbon sequestration. Serpentinization in these rocks enhances their reactivity, facilitating mineral carbonation and making them prime candidates for CCS applications. Data interpretation confirms that the Kolaka ultramafic rocks exhibit mineralogical and geochemical properties for long-term carbon storage. Secondary carbonate minerals such as magnesite and brucite along serpentine veins and fractures suggest active carbonation processes. Additionally, the study underscores the significance of magnesium in ultramafic rocks, as it reacts efficiently with CO<sub>2</sub> to form stable carbonates, thus offering a promising geological solution for mitigating atmospheric carbon levels. Overall, this research contributes valuable insights into the mineral potential of ultramafic rocks for carbon storage and emphasizes the critical role of geological formations in global climate change mitigation efforts. Analyzing these rocks' carbonation potential sets a foundation for future CCS initiatives, particularly in regions with prevalent ultramafic complexes.

## Acknowledgments

The authors express their gratitude to the Ministry of Higher Education and the Research and Community Service Institute (LPPM) of Universitas Sembilanbelas November for the funding support provided for this research under the DRTPM Diktiristek Penelitian Dosen Pemula (PDP) scheme for the 2024 period.

## References

- Andreani, M., Luquot, L., Gouze, P., Godard, M., Hoisé, E. & Gibert, B. 2009. Experimental Study of Carbon Sequestration Reactions Controlled by the Percolation of CO<sub>2</sub>-Rich Brine through Peridotites. *Environmental science & technology*, 43. 1226-31. <https://doi.org/10.1021/es8018429>
- Asadnabizadeh, M. 2019. Analysis of Internal Factors of the Swing States in the International Climate Change Negotiations: A Case Study of Poland in COP24. *American Journal of Climate Change*, 08(02). 263-283. <https://doi.org/10.4236/ajcc.2019.82015>
- Bide, T., Styles, M. & Naden, J. 2014. An assessment of global resources of rocks as suitable raw materials for carbon capture and storage by mineralisation. *Applied Earth Science IMM Transactions section B*, 123. 179-195. <https://doi.org/10.1179/1743275814Y.0000000057>
- Chang, L., Zhang, R. & Wang, C. 2022. Evaluation and Prediction of Landslide Susceptibility in Yichang Section of Yangtze River Basin Based on Integrated Deep Learning Algorithm. *Remote Sensing*, 14(11). 2717.
- Erlania, E., Nirmala, K. & Soelistyowati, D. T. 2013. Penyerapan karbon pada budidaya rumput laut *Kappaphycus alvarezii* dan *Gracilaria gigas* di Perairan Teluk Gerupuk, Lombok Tengah, Nusa Tenggara Barat. *Jurnal Riset Akuakultur*, 8(2). 287-297. <https://doi.org/10.15578/jra.8.2.2013.287-297>
- Hansen, L. D., Dipple, G. M., Gordon, T. M. & Kellett, D. A. 2005. CARBONATED SERPENTINITE (LISTWANITE) AT ATLIN, BRITISH COLUMBIA: A GEOLOGICAL ANALOGUE TO CARBON DIOXIDE SEQUESTRATION. *The Canadian Mineralogist*, 43(1). 225-239. <https://doi.org/10.2113/gscanmin.43.1.225>
- Harrison, A., Mavromatis, V., Oelkers, E. & Bénézech, P. 2018. Solubility of the hydrated Mg-carbonates nesquehonite

- and dypingite from 5 to 35 °C: Implications for CO<sub>2</sub> storage and the relative stability of Mg-carbonates. *Chemical Geology*, 504. <https://doi.org/10.1016/j.chemgeo.2018.11.003>
- Höhne, N., Gidden, M. J., Den Elzen, M., Hans, F., Fyson, C., Geiges, A., Jeffery, M. L., Gonzales-Zuñiga, S., Mooldijk, S., Hare, W. & Rogelj, J. 2021. Wave of net zero emission targets opens window to meeting the Paris Agreement. *Nature Climate Change*, 11(10). 820-822. <https://doi.org/10.1038/s41558-021-01142-2>
- Irzon, R., Hanang, S. & Sam, P. 2024. Prospecting CCS Project in Indonesia: A Case Study in Meratus Mountains, South Borneo. *Jurnal Geologi dan Sumberdaya Mineral*, 25(1). 31-40. <https://doi.org/10.33332/jgsm.geologi.v25i1.784>
- Jaya, R. I. M. C., Juarsan, L. I., Haraty, S. R., Pramadana, R. & Hasria 2024a. Serpentine Paragenesis in Ultramafic Rocks of the Baula - Pomalaa Ophiolite Complex, Southeast Sulawesi, Indonesia. *Journal of Geology and Mineral Resources*, 25(2). 95-106. <https://doi.org/10.33332/jgsm.geologi.v25i2.761>
- Jaya, R. I. M. C., Juarsan, L. I., Masri, Rubaiyn, A., Syahrul, Neni, Ramadani, S. & Hasria 2024b. Petrochemistry of Ultramafic Rock in Baula-Pomalaa Ophiolite Complex, Southeast Sulawesi, Indonesia. *Journal of Geoscience, Engineering, Environment, and Technology*, 9(1). 44-51. <https://doi.org/10.25299/jgeet.2024.9.1.14491>
- Jompa, J. & Murdiyarso, D. 2022. Rehabilitasi Kawasan Pesisir untuk Adaptasi Perubahan Iklim: Peran kunci mangrove dalam Nationally Determined Contributions, Working Paper 12. Bogor, Indonesia, CIFOR-ICRAF.p. <https://doi.org/https://doi.org/10.17528/cifor-icraf/008792>
- Kadarusman, A., Miyashita, S., Maruyama, S., Parkinson, C. D. & Ishikawa, A. 2004. Petrology, geochemistry and paleogeographic reconstruction of the East Sulawesi Ophiolite, Indonesia. *Tectonophysics*, 392(1-4). 55-83. <https://doi.org/10.1016/j.tecto.2004.04.008>
- Kelemen, P., Benson, S., Pilorgé, H., Psarras, P. C. & Wilcox, J. 2019. An Overview of the Status and Challenges of CO<sub>2</sub> Storage in Minerals and Geological Formations. *Frontiers in Climate*, 1. <https://doi.org/10.3389/fclim.2019.00009>
- Kelemen, P., McQueen, N., Wilcox, J., Renforth, P., Dipple, G. & Paukert Vankeuren, A. 2020. Engineered carbon mineralization in ultramafic rocks for CO<sub>2</sub> removal from air: Review and new insights. *Chemical Geology*, 550. 119628. <https://doi.org/10.1016/j.chemgeo.2020.119628>
- Luu, K., Schoenball, M., Oldenburg, C. & Rutqvist, J. 2022. Coupled Hydromechanical Modeling of Induced Seismicity From CO<sub>2</sub> Injection in the Illinois Basin. *Journal of Geophysical Research: Solid Earth*, 127. <https://doi.org/10.1029/2021JB023496>
- Matter, J. M., Stute, M., Snæbjörnsdóttir, S., Oelkers, E. H., Gislason, S. R., Aradóttir, E. S., Sigfusson, B., Gunnarsson, I., Sigurdardóttir, H., Gunnlaugsson, E., Axelsson, G., Alfredsson, H. A., Wolff-Boenisch, D., Mesfin, K., Fernandez de la Reguera Taya, D., Hall, J., Dideriksen, K. & Broecker, W. S. 2016. Rapid carbon mineralization for permanent disposal of anthropogenic carbon dioxide emissions. *Science*, 352(6291). 1312-4. <https://doi.org/10.1126/science.aad8132>
- Maulana, A., Christy, A. G. & Ellis, D. J. 2015. Petrology, geochemistry and tectonic significance of serpentinitized ultramafic rocks from the South Arm of Sulawesi, Indonesia. *Geochemistry*, 75(1). 73-87. <https://doi.org/10.1016/j.chemer.2014.09.003>
- Medhaug, I., Stolpe, M. B., Fischer, E. M. & Knutti, R. 2017. Reconciling controversies about the 'global warming hiatus'. *Nature*, 545(7652). 41-47. <https://doi.org/10.1038/nature22315>
- Power, I., Wilson, S. & Dipple, G. 2013. Serpentinite Carbonation for CO<sub>2</sub> Sequestration. *Elements*, 9. 115-121. <https://doi.org/10.2113/gselements.9.2.115>
- Punnam, P., Krishnamurthy, B. & Surasani, V. 2022. Influence of Caprock Morphology on Solubility Trapping during CO<sub>2</sub> Geological Sequestration. *Geofluids*, 2022. 1-15. <https://doi.org/10.1155/2022/8016575>
- Rigopoulos, I., Delimitis, A., Ioannou, I., Efstathiou, A. M. & Kyratsi, T. 2018. Effect of ball milling on the carbon sequestration efficiency of serpentinitized peridotites. *Minerals Engineering*, 120. 66-74. <https://doi.org/https://doi.org/10.1016/j.mineng.2018.02.011>
- Rogelj, J., den Elzen, M., Höhne, N., Fransen, T., Fekete, H., Winkler, H., Schaeffer, R., Sha, F., Riahi, K. & Meinshausen, M. 2016. Paris Agreement climate proposals need a boost to keep warming well below 2 °C. *Nature*, 534(7609). 631-9. <https://doi.org/10.1038/nature18307>
- Simandjuntak, T. O., Suroño & Sukido. 1993. *Peta Geologi Lembar Kolaka, Sulawesi*. Bandung: Pusat Penelitian dan Pengembangan Geologi.
- Snæbjörnsdóttir, S. Ó., Sigfusson, B., Marieni, C., Goldberg, D., Gislason, S. & Oelkers, E. 2020. Carbon dioxide storage through mineral carbonation. *Nature Reviews Earth & Environment*, 1. 1-13. <https://doi.org/10.1038/s43017-019-0011-8>
- Steinhorsdóttir, K., Dipple, G. M., Cutts, J. A., Turvey, C. C., Milidragovic, D. & Peacock, S. M. 2022. Formation and Preservation of Brucite and Awaruite in Serpentinized and Tectonized Mantle in Central British Columbia: Implications for Carbon Mineralization and Nickel Mining. *Journal of Petrology*, 63(11). <https://doi.org/10.1093/petrology/egac100>
- Streckeisen, A. 1976. To each plutonic rock its proper name. *Earth-Science Reviews*, 12(1). 1-33. [https://doi.org/10.1016/0012-8252\(76\)90052-0](https://doi.org/10.1016/0012-8252(76)90052-0)
- Sufriadin, Widodo, S., Thamrin, M., Maulana, A., Ito, A. & Otake, T. 2020. The nature of ultramafic rocks from Sulawesi, Indonesia and their suitability for CO<sub>2</sub> sequestration. *IOP Conference Series: Earth and Environmental Science*, 589(1). 012024. <https://doi.org/10.1088/1755-1315/589/1/012024>
- Syahrul. 2017. Studi Petrogenesis Dan Mineralisasi Kompleks Batuan Ultramafik Daerah Sopura, Kabupaten Kolaka, Provinsi Sulawesi Tenggara. Institut Teknologi Bandung.
- Tolliver, C., Keeley, A. R. & Managi, S. 2019. Green bonds for the Paris agreement and sustainable development goals. *Environmental Research Letters*, 14(6). 064009. <https://doi.org/10.1088/1748-9326/ab1118>
- Triana, K. & Wahyudi, J. 2020. Sea level rise in Indonesia: The drivers and the combined impacts from land subsidence. *ASEAN Journal on Science and Technology for Development*, 37(3). 3.
- Trivedi, A., Pyasi, S. K. & Galkate, R. V. 2019. Impact of Climate Change Using Trend Analysis of Rainfall, RRL AWBM Toolkit, Synthetic and Arbitrary Scenarios. *Current Journal of Applied Science and Technology*, 38(6). 1-18. <https://doi.org/10.9734/cjast/2019/v38i630431>

- Tutolo, B. M., Luhmann, A. J., Kong, X. Z., Saar, M. O. & Seyfried, W. E., Jr. 2014. Experimental observation of permeability changes in dolomite at CO<sub>2</sub> sequestration conditions. *Environ Sci Technol*, 48(4). 2445-52. <https://doi.org/10.1021/es4036946>
- Warwick, P. D. & Zhu, Z.-L. 2012. New insights into the nation's carbon storage potential. *Eos, Transactions, American Geophysical Union*, 93(26). 241-242.

<https://doi.org/10.1029/2012EO260001>

Whitney, D. L. & Evans, B. W. 2009. Abbreviations for names of rock-forming minerals. *American Mineralogist*, 95(1). 185-187. <https://doi.org/10.2138/am.2010.3371>



© 2025 Journal of Geoscience, Engineering, Environment and Technology. All rights reserved. This is an open access article distributed under the terms of the CC BY-SA License (<http://creativecommons.org/licenses/by-sa/4.0/>).